Surfing beta burst waveforms to improve motor imagery-based BCI

Sotirios Papadopoulos, Ludovic Darmet, Maciej J Szul, Marco Congedo, James J Bonaiuto, Jérémie Mattout

Imaging Neuroscience
an open access journal

Research Article

Surfing beta burst waveforms to improve motor imagery-based BCI

Sotirios Papadopoulos[a,b,c], Ludovic Darmet[a,b,c], Maciej J. Szul[a,c], Marco Congedo[d], James J. Bonaiuto[a,c,*], Jérémie Mattout[a,b,*]

[a]University Lyon 1, Lyon, France
[b]Lyon Neuroscience Research Center, CRNL, INSERM, U1028, CNRS, UMR 5292, Lyon, France
[c]Institut des Sciences Cognitives Marc Jeannerod, CNRS, UMR 5229, Lyon, France
[d]GIPSA-lab, University Grenoble Alpes, CNRS, Grenoble-INP, Grenoble, France

*These authors contributed equally

Corresponding Author: Sotirios Papadopoulos (sotirios.papadopoulos@univ-lyon1.fr)

ABSTRACT

Our understanding of motor-related, macroscale brain processes has been significantly shaped by the description of the event-related desynchronization (ERD) and synchronization (ERS) phenomena in the mu and beta frequency bands prior to, during, and following movement. The demonstration of reproducible, spatially- and band-limited signal power changes has, consequently, attracted the interest of non-invasive brain-computer interface (BCI) research for a long time. BCIs often rely on motor imagery (MI) experimental paradigms that are expected to generate brain signal modulations analogous to movement-related ERD and ERS. However, a number of recent neuroscience studies has questioned the nature of these phenomena. Beta band activity has been shown to occur, on a single-trial level, in short, transient, and heterogeneous events termed bursts rather than sustained oscillations. In a previous study, we established that an analysis of hand MI binary classification tasks based on beta bursts can be superior to beta power in terms of classification score. In this article, we elaborate on this idea, proposing a signal processing algorithm that is comparable to- and compatible with state-of-the-art techniques. Our pipeline filters brain recordings by convolving them with kernels extracted from beta bursts and then applies spatial filtering before classification. This data-driven filtering allowed for a simple and efficient analysis of signals from multiple sensors, thus being suitable for online applications. By adopting a time-resolved decoding approach, we explored MI dynamics and showed the specificity of the new classification features. In accordance with previous results, beta bursts improved classification performance compared to beta band power, while often increasing information transfer rate compared to state-of-the-art approaches.

Keywords: beta bursts, brain–computer interface (BCI), decoding, electro-encephalography (EEG), motor imagery (MI)

1. INTRODUCTION

Time-locked changes in induced power within specific frequency bands, originally described in a number of seminal studies in motor neuroscience (Pfurtscheller, 1981; Pfurtscheller & Berghold, 1989; Pfurtscheller & Lopes da Silva, 1999), have long influenced the way in which we interpret macroscale recordings of brain activity such as those provided by electroencephalography (EEG). These studies have revealed a gradual reduction in brain signal power during an ongoing movement or motor imagery (MI) task in the mu (~8–12 Hz) (Neuper et al., 2006; Pfurtscheller et al., 1997, 2006; Pfurtscheller & Lopes da Silva, 1999) and beta (~13–30 Hz) (Pfurtscheller et al., 1997; Pfurtscheller & Lopes da Silva, 1999) frequency bands relative to baseline activity. This phenomenon is termed event-related desynchronization (ERD).

Received: 23 July 2024 Revision: 18 October 2024 Accepted: 1 November 2024 Available Online: 25 November 2024

The same studies have, moreover, described a relative-to-baseline increase in power in the beta band shortly following the end of the movement or MI (Alayrangues et al., 2019; Neuper et al., 2006; Pfurtscheller et al., 1996), known as event-related synchronization (ERS). These phenomena are especially marked over cortical areas contralateral to the real or imagined movement (Kobler et al., 2020; Little et al., 2019; Makeig et al., 2000; Pfurtscheller & Berghold, 1989; Pfurtscheller & Neuper, 1997; Seeber et al., 2016; Zich et al., 2023), and their topographies approximately match the somatotopic organization of the sensorimotor cortices (Gordon et al., 2023; Natraj et al., 2022; Penfield & Rasmussen, 1950). Taken together, these observations have given rise to the hypothesis that the ERD is an indication of brain processes pertaining to movement preparation and execution while the ERS is an indication of processes related to movement completion (Kilavik et al., 2013).

Given the reproducibility of the spatial and frequency specificity of the ERD and ERS, these neural markers are often exploited by non-invasive BCI applications, especially those that are based on MI paradigms (Jayaram & Barachant, 2018; Tangermann et al., 2012). Such paradigms, designed to reproduce consistent time-locked signal modulations, normally rely on transforming the recordings in the time-frequency domain (TF) (Brodu et al., 2011; Bruns, 2004; Herman et al., 2008) and then applying spatial filtering, most commonly using the common spatial pattern algorithm (CSP) (Blankertz et al., 2007; Koles, 1991; Müller-Gerking et al., 1999). This chain of signal transformations is expected to increase signal-to-noise ratio by extracting signal power in specific time windows and frequency bands of interest, and also to maximize the spatial disparity among different MI classes (e.g., "left" or "right" hand, or "feet"), thus improving classification results and/or allowing for decoding of multiple commands with distinct signal features (Lotte, 2014; Lotte et al., 2018).

Although the ERD and ERS are consistently observed across subjects and recording modalities, their nature is not clear. Based on the assumption of amplitude modulation of sustained oscillations, these patterns are the result of signal power averaging in the TF domain over multiple trials. However, converging evidence suggests that, on the contrary, beta band activity occurs in short events termed bursts (Coleman et al., 2024; Jones, 2016; Little et al., 2019; Lundqvist et al., 2016, 2024; Shin et al., 2017; Torrecillos et al., 2018; Wessel, 2020; West et al., 2023) on the single-trial level, therefore questioning the functional role of ERD and ERS altogether, at least within the beta band. Beta burst rate has been shown to be more behaviorally relevant in motor processes (Enz et al., 2021; Hannah et al., 2020; Little et al., 2019; Rayson et al., 2023; Soh et al., 2021; Szul et al., 2023; Wessel, 2020) than averaged beta band power. Additionally, recent studies have shown that beta bursts are not a unitary phenomenon but rather constitute heterogeneous events (Szul et al., 2023) with different functions, alluded to by the differential modulation of their rate and shape depending on task conditions (Langford et al., 2023; Papadopoulos et al., 2024) or movement phase (Rayson et al., 2023; Szul et al., 2023). As such, beta bursts have the potential to be a more sensitive marker of brain processes during real or imagined movements on the single-trial level.

To test this hypothesis, in a previous study we examined six open, benchmark MI EEG datasets, which we also analyzed here. In that study, we analyzed the activity of channels C3 and C4 during binary classification tasks of hand MI, that is, "left" versus "right" hand under the assumption that beta burst activity modulations during MI should resemble those observed during real movements of the upper limbs. We demonstrated that the waveform-resolved beta burst rate is superior to beta band power changes and alternative beta burst representations in terms of classification (Papadopoulos et al., 2024). Briefly, we adopted a nested cross-validation approach in order to identify the optimal waveforms for maximizing classification score. This was done by first iterating over different data samples, finding multiple beta burst waveforms from each sample, then treating each distinct waveform as a point process, and computing the corresponding burst rate. The best (in terms of classification score) combination of waveform-specific burst rates was then selected based on cross-validation, before being tested on a previously unseen validation sample in each iteration of the nested cross-validation. The major limitation of that study was the algorithm's computational complexity, which was unsuitable to be potentially translated to real-time implementations, and also compelled us to restrict the analysis only to channels C3 and C4 assuming that they capture brain signal modulations that are relevant to the task.

In this article, we streamline our approach. We develop an algorithm that is computationally efficient and can analyze an arbitrary number of recorded signals, thus being comparable to state-of-the-art techniques. Beta burst waveforms, whose rate is expected to be maximally modulated during the trial period compared to baseline, are identified in calibration data. These bursts are used as data-driven kernels that filter the signals from all recording channels in the time domain. The convolved signals are then spatially filtered with CSP, and the spatial features are used as classification features. We re-analyze the activity during "left" and "right" hand MI of the same open EEG datasets and also a recently-published composite EEG dataset, now in a time-resolved fashion. We show that classification features based on waveform-resolved beta

burst rate offer better decoding performance and improve the decoding speed versus accuracy trade-off when compared to standard band-limited, power-based classification features.

2. METHODS

2.1. Datasets

We analyzed the recordings of six open EEG MI benchmark datasets available through the MOABB (Aristimunha et al., 2023; Jayaram & Barachant, 2018) project: BNCI 2014-001 (Tangermann et al., 2012), BNCI 2014-004 (Leeb et al., 2007), Cho 2017 (Cho et al., 2017), Munich MI (Grosse-Wentrup 2009) (Grosse-Wentrup et al., 2009), Weibo 2014 (Yi et al., 2014), and Zhou 2016 (Zhou et al., 2016), and the recordings of a composite open EEG dataset that became recently available (Dreyer et al., 2023) referred to hereafter as Dreyer 2023. All datasets comprise a number of subjects with recordings corresponding to multiple trials of two or more randomly chosen, sustained kinesthetic MI commands, each performed following the appearance of a visual cue on a screen (Table 1). For our analysis we only considered trials corresponding to the "left hand" or "right hand" classes. No new data were collected in this work. Please refer to each study for details on approval of local authorities and informed consent of the participants.

2.2. Pre-processing

The epoched recordings of each subject were loaded using the MOABB python package (v0.4.6, class LeftRightImagery; parameters: t_{min} and t_{max} as indicated in Table 1), and were filtered with a low pass cutoff of 120 Hz (parameters: f_{min} = 0, f_{max} = 120; default MNE (Gramfort et al., 2013) zero-phase FIR filter designed with the windowed approach and transition bandwidth of 25% of the low pass frequency). Because the sampling frequency of the Weibo 2014 recordings is 200 Hz, we set the low pass cutoff to 95 Hz for this dataset. Finally, we used the autoreject python package (Jas et al., 2017) (v0.4.0, function get_rejection_threshold, default parameters) in order to remove noisy trials.

2.3. Burst detection and kernel selection

In order to select kernels for convolving the data from all channels, we first detected bursts, after applying the pre-processing steps described above within a dataset-specific cluster of channels above the sensorimotor cortex (Papadopoulos et al., 2024). We applied a time-frequency (TF) decomposition in the 1–43 Hz range on each selected channel separately, using the superlets algorithm (Moca et al., 2021) (parameters: o_{min} = 1, o_{max} = 40, c = 4) with a frequency resolution of 0.5 Hz. We noted narrow-band, high-power artifacts at approximately 25–30 Hz when inspecting the TF of the Cho 2017, Dreyer 2023 and Munich MI (Grosse-Wentrup 2009) datasets, possibly attributable to power-line sub-harmonics or some other source of electronic interference. This noise interferes with the burst detection step; therefore, we included an extra pre-processing step, prior to trial rejection, based on a custom implementation of the ZapLine algorithm (de Cheveigné, 2020) from the

Table 1. Dataset attributes.

Dataset	# Subjects	# Channels	# Trials	Baseline period (s)	Task period (s)	Post-task period (s)
BNCI 2014-001	9	22	288 217 – 288 (243)	-1.0 – 0.0	0.0 – 4.0	4.0 – 5.5
BNCI 2014-004	9	3	680 – 760 (720) 269 – 621 (411)	-1.0 – 0.0	0.0 – 4.5	4.5 – 6.5
Cho 2017	49	64	200 – 240 (200) 38 – 237 (159)	-1.0 – 0.0	0.0 – 3.0	3.0 – 5.0
Dreyer 2023	87	27	160 – 240 (240) 23 – 240 (192)	-1.0 – 0.0	0.0 – 5.0	5.0 – 6.0
Munich MI (Grosse-Wentrup 2009)	10	128	300 109 – 278 (200)	-1.0 – 0.0	0.0 – 7.0	7.0 – 9.0
Weibo 2014	10	64	140 – 160 (160) 31 – 160 (132)	-1.0 – 0.0	0.0 – 4.0	4.0 – 5.0
Zhou 2016	4	14	290 – 319 (295) 114 – 280 (150)	-1.0 – 0.0	0.0 – 5.0	5.0 – 7.0

The lines in the fourth column indicate the original number of trials per subject (or the range in case this number was different between subjects), and the range of remaining trials across all subjects following trial rejection. Numbers in parentheses indicate the median number of trials.

meegkit python package (v0.1.3, dss_line function) to remove these artifacts (Supplementary Fig. 1).

Then, we detected bursts within the beta frequency range (15–30 Hz) from each TF matrix channel and used their temporal location to extract their waveforms from the raw time series within a fixed time window of 260 ms as described in detail in Szul et al. (2023) and adapted for the analyzed datasets in Papadopoulos et al. (2024). In summary, the burst detection algorithm iteratively identifies the highest amplitude of a TF matrix and models it as two-dimensional Gaussian taking into account the full-width at half-maximum (FWHM) of the peak amplitude along the dimensions of time and frequency. Then, the time point of the burst's peak amplitude is used to look for the centering point of each waveform in the low-passed EEG signal. This corresponds to the signal's minimum phase point around the peak provided that it occurs within 30 ms prior to or following this peak. Based on the FHWM of the average lagged coherence value across the beta frequency band, a time window of 260 ms is used to extract the burst waveform. Finally, the 2D Gaussian is subtracted from the TF matrix and the TF residual is used in the next algorithm iteration. The process stops when no amplitude peak exceeds the noise floor of two standard deviations across the whole TF matrix. For more details regarding the burst detection step, we refer the readers to previous work from our group (Szul et al., 2023).

As the number of detected bursts per subject is large, we randomly sampled 10% of the trials of each participant per dataset and created a matrix that contained the waveforms of all detected bursts regardless of the trial class ("left" or "right" hand) for a given dataset, corresponding to approximately 100,000 to 2,000,000 bursts depending on the dataset. Due to the large number of subjects of the Dreyer 2023 dataset we restricted the random sample to 5% of each subject's trials. The sample sizes were selected such that enough data were provided to the PCA in order for the selected kernels (see below) to be stable over multiple iterations of the random sampling (Supplementary Fig. 2), while as many data as possible were retained for performing the rest of the analysis. Then, after robust scaling (scikit-learn package (Pedregosa et al., 2011), v1.0.2), we reduced the time dimension of the waveforms using principal component analysis (PCA) (Shlens, 2014) (scikit-learn package, v1.0.2).

We used the PCA score of each waveform detected from electrodes C3 and C4 (or equivalently channels 43 and 44 for the Munich MI (Grosse-Wentrup 2009) dataset), which is a metric of the difference between any waveform and the average shape of all bursts contained in the matrix provided as input to PCA. We defined an index of lateralized modulation of the average-per-axis PCA score I_m:

$$I_m = \left|\left(u_{ipsi}^{C3} - u_{contra}^{C4}\right) - \left(u_{ipsi}^{C4} - u_{contra}^{C3}\right)\right|, m \in \{2,...,9\}$$

$$u = \left|\widehat{\text{score}}_{trial\ \ period} - \widehat{\text{score}}_{baseline}\right|$$

where ipsi (contra) refers to bursts recorded from channels C3 / C4 during a left / right (right / left) hand MI (Fig. 1a).

This index measures the inter-hemispheric difference of the average waveform shape between the baseline and trial periods. Its values span the range $[0,\infty)$ and higher values indicate greater discrepancies between hemispheres and the two recording periods.

Based on observations from our previous study (Papadopoulos et al., 2024), we computed I_m among components 2 to 9 in order to find three PCA axes that maximized this metric. We did not take into account the first component because it likely describes the temporal skew of the bursts (Papadopoulos et al., 2024; Szul et al., 2023). Finally, we divided the score range of each of the three selected axes in seven equally spaced groups, each group corresponding to a set of "similarly shaped" bursts. We kept the two groups per axis that lie further away from the origin (score equal to 0) and, by computing the Euclidean-average waveform of bursts within each group, we identified two kernels per axis. As such, we identified six kernels per dataset corresponding to burst waveforms whose rates were expected to be maximally modulated during the task, compared to baseline.

2.4. Feature extraction

For each subject we applied the pre-processing, burst detection, and kernel selection steps described above (pre-processing was applied to all available recording channels). Then, we convolved the EEG recordings with the corresponding kernels, thus computing a proxy of the waveform-resolved burst rate per kernel. The temporally convolved, epoched data were then spatially filtered using the CSP algorithm (MNE package, v1.5.1, function CSP, parameters: n_components = 4, transform_into = "average_power"). Finally, we concatenated all 24 spatial features into a single vector for each trial (Fig. 1b).

To compare with, we also used standard approaches to compute spatial features of band-limited power modulations. After pre-processing, we independently filtered the epoched data in the mu (6–15 Hz), beta (15–30 Hz), or both the mu and beta (6–30 Hz) bands, using either a single filter or a filter bank approach. Then, the filtered data served as inputs to the CSP algorithm (using the already

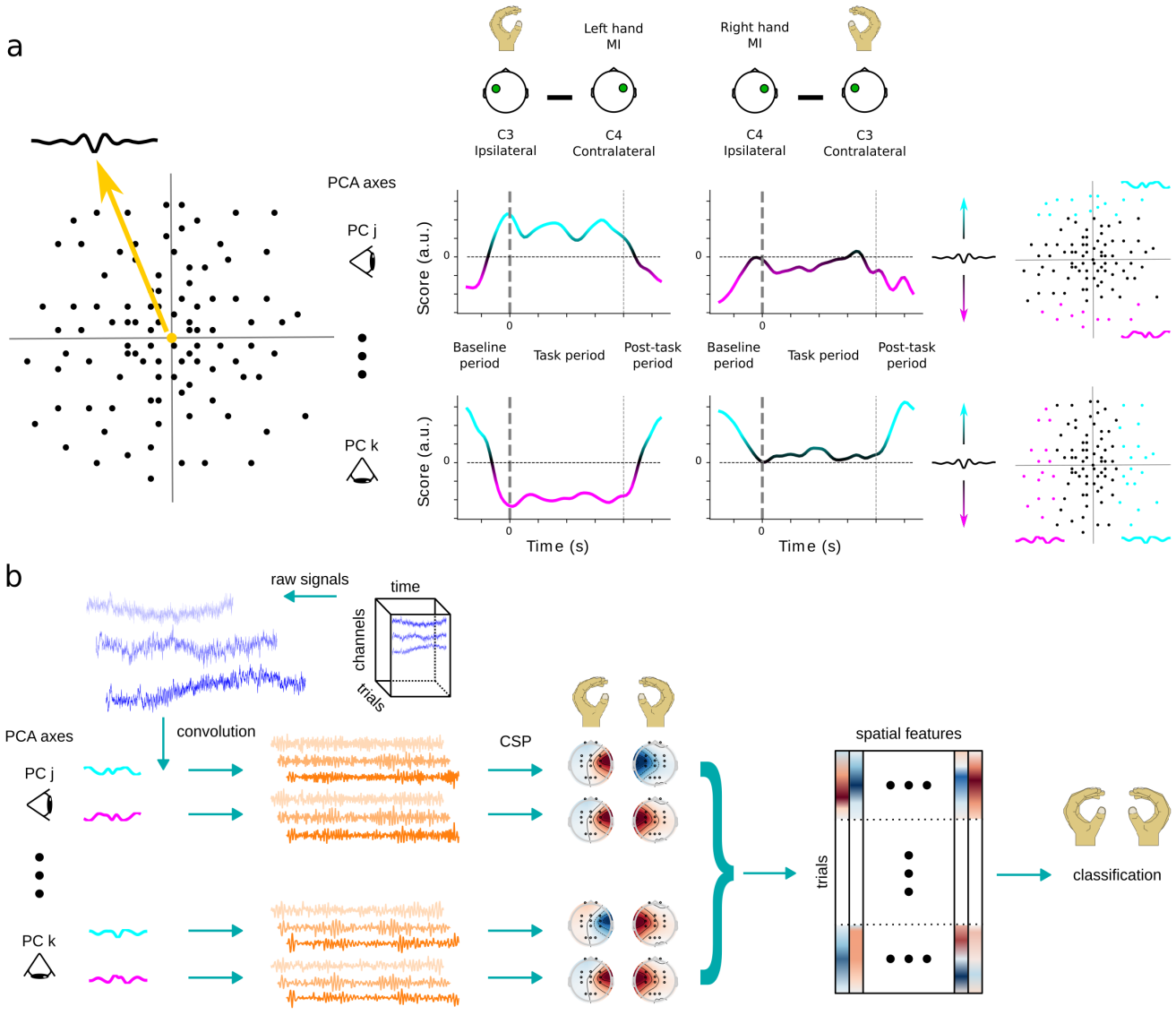

Fig. 1. Illustration of methodology for computing classification features based on the convolution of raw signals with beta burst waveform kernels. (a) After randomly sampling the recording trials of all subjects within any dataset, the beta burst waveforms are analyzed using PCA. This constructs a high-dimensional space whose origin corresponds to the shape of the average waveform or equivalently a score equal to 0, and each axis defines a different axis of waveform variation. By only considering the beta bursts of channels C3 and C4 that occur at any point in time, the lateralization modulation index I_m dynamically identifies the expected deviation of the average waveform shape from the overall average shape for each PCA axis. The axes that maximize I_m are identified, the bursts are projected on these axes, split in groups of similarly shaped waveforms and the average waveform shapes of the two extrema are computed. (b) The raw signals of all recording channels of each dataset are independently convolved with each selected waveform from (a), resulting in distinctly temporally filtered copies of the signals. Each copy is then spatially filtered using the CSP algorithm, and finally all spatial features are concatenated in a single matrix that is provided as input to the classifier.

described parameters), resulting in four spatial features per filter in the former case. For the filter bank approach, we split either frequency range in non-overlapping filter banks with a frequency span of 3 Hz per filter. As such, we defined three filters for the mu band (6–9 Hz, 9–12 Hz, 12–15 Hz), five filters for the beta band (15–18 Hz, 18–21 Hz, 21–24 Hz, 24–27 Hz, 27–30 Hz), and eight filters for the mu-beta band (6–9 Hz, 9–12 Hz, 12–15 Hz, 15–18 Hz, 18–21 Hz, 21–24 Hz, 24– 27 Hz, 27–30 Hz). Then, we again used CSP and concatenated all spatial features of each filter bank, resulting in 12, 20, and 32 spatial features respectively per trial.

2.5. Classification

We used a repeated (n = 10), 5-fold cross-validation procedure to estimate the decoding score using linear discriminant analysis (LDA) (Tharwat et al., 2017; Vidaurre

et al., 2011) (scikit-learn, v1.0.2) as a classifier. We adopted a time-resolved decoding paradigm, using both an incremental and a sliding time window. In the first case, we started with a 100 ms time window and repeated the classification procedure by incrementing this window by 100 ms at a time. The baseline period was considered separately from the trial period. In the latter case, we used 1 second long sliding time windows which moved in 50 ms increments. Decoding scores were based on the area under the curve (AUC) of the receiver operating characteristic (scikit-learn, v1.0.2). All numeric computations were based on the numpy python package (v1.21.6; Harris et al., 2020) and an environment running python (v3.10).

2.6. Information transfer rate

Information transfer rate (Arslan & Sinha, 2024; Sadeghi & Maleki, 2019) was defined as:

$$ITR = \frac{1-H}{T}$$

$$H = -p(t)log_2p(t) - (1-p(t))log_2(1-p(t))$$

where the binary entropy function H depends on the average accuracy probability at any time window $p(t)$, and T corresponds to the maximum recording time required by each time window in seconds. T was shifted such that all time values are positive, that is, using the absolute time starting from the beginning of the baseline period (Table 1) when using a sliding window and when considering the baseline period using an incremental time window. The values of this metric span the range $[0,10]$ when using an incremental window decoding approach and $[0,20]$ when using a sliding window. Large values indicate a better trade-off between decoding accuracy and decoding speed.

2.7. Statistical analysis

On the dataset level, we performed pairwise comparisons of the across-subject average decoding score corresponding to the beta burst convolution spatial features and each of the spatial features of the band-limited power modulations. These comparisons were based on threshold-free cluster-based permutation ($n = 2^{13}$) tests (MNE package, v1.5.1, function permutation_cluster_test, parameters: threshold = dict(start = 0, step = 0.2), tail = 1) that were subsequently thresholded at significance level of a = 0.05 for visualization purposes.

To estimate, on the population level, any statistical differences between the maximum classification scores obtained using different feature extraction pipelines during the trial period, we compared the scores of the beta burst convolution pipeline against those based on classical filtering pipelines. We used a linear mixed model with across-trials average classification score as the dependent variable setting the number of trials as prior weights, the type of classification feature as a fixed effect, and subject nested within dataset as random intercepts. We implemented similar models to compare the time required to achieve the maximum classification score per feature extraction pipeline, and also the maximum ITR and time needed to reach it. In the latter two cases, we first transformed the values to logarithmic scale in order to ensure normality of the residuals. Statistical analyses were conducted using R (v4.1.2) and lme4 (v1.1-31; Bates et al., 2015). Fixed effects were assessed using type II Wald X 2 tests using car (v3.1-1; Fox & Weisberg, 2019). Pairwise Tukey-corrected follow-up tests were carried out using estimated marginal means from the emmeans package (v.1,8,7; Lenth, 2023).

3. RESULTS

3.1. Classification

In summary, we have employed seven freely available datasets of EEG recordings from subjects performing left and right hand MI. Within each dataset, we detected beta bursts for each subject within electrode clusters over the left and right sensorimotor cortex and then randomly sampled 10% of the trials containing these bursts (the sample size was limited to 5% for the Dreyer 2023 dataset). We applied PCA to the matrix of all burst waveforms and defined a modulation index I_m in order to find burst waveform shapes whose lateralized rates were expected to be maximally modulated between the baseline and trial periods. These waveforms were then employed as kernels for convolving the EEG data in time domain before applying spatial filtering with CSP. Finally, all spatial features were combined and served as input for LDA, in order to classify “left” versus “right” hand MI. We also performed classification by applying standard temporal filtering techniques before applying spatial filtering with CSP, using either a single filter or a filter bank in the mu (6–15 Hz), beta (15–30 Hz), and mu-beta (6–30 Hz) frequency bands. We estimated the time-resolved decoding score per subject of each dataset for each classification feature using both an incremental and a sliding decoding window (see Section 2 for details).

Across all datasets, the average decoding accuracy obtained using the proposed methodology based on beta bursts outperformed the results based on standard beta band filtering irrespective of the filtering (single filter or filter bank) or the windowing (incremental or sliding)

technique during most of the recording time (Fig. 2a; Supplementary Fig. 3a). Within each dataset, the across-subjects average score obtained by beta bursts was higher than that of any beta band filtering technique, usually shortly after the beginning of the trial or towards its end (Fig. 2b–h; Supplementary Fig. 3b–h). Exceptions to this finding when using an incremental window were the BNCI 2014-001 dataset, for which all features produced equivalent results (Fig. 2c; Supplementary Fig. 3c), and the Weibo 2014 dataset, for which mu-beta filtering outperformed beta bursts (Fig. 2g; Supplementary Fig. 3g). Threshold-free cluster-based permutation tests (see Section 2) revealed a significant cluster of increased accuracy for beta bursts compared to either beta filtering technique during most of the recording time or following the trial onset for each windowing (incremental or sliding) technique respectively (Fig. 2a; Supplementary Fig. 3a). Within each dataset, we found clusters similar to those of the population average for the Dreyer 2023 dataset (Fig. 2e; Supplementary Fig. 3e). The across-subjects average score obtained by beta bursts was higher than that of any beta band filtering technique shortly after the beginning of the trial for the BNCI 2014-001 and Cho 2017 datasets (Fig. 2b, d; Supplementary Fig. 3b, d). For the rest of the datasets (BNCI 2014-004, Munich MI (Grosse-Wentrup 2009), Weibo 2014, Zhou 2016) no differences were observed among the beta bursts and either beta band filtering method. Overall, in terms of classification accuracy, we observed an improvement with beta bursts over beta power on the population level and in 5/7 (4/7) datasets, with clusters of statistically significant differences arising on the population level and in 3/7 (2/7) datasets when using an incremental (sliding) window.

We did not observe such clear differences when comparing the beta bursts and mu-beta filtering decoding scores. On the population level, when using an incremental time window, average beta burst convolution results

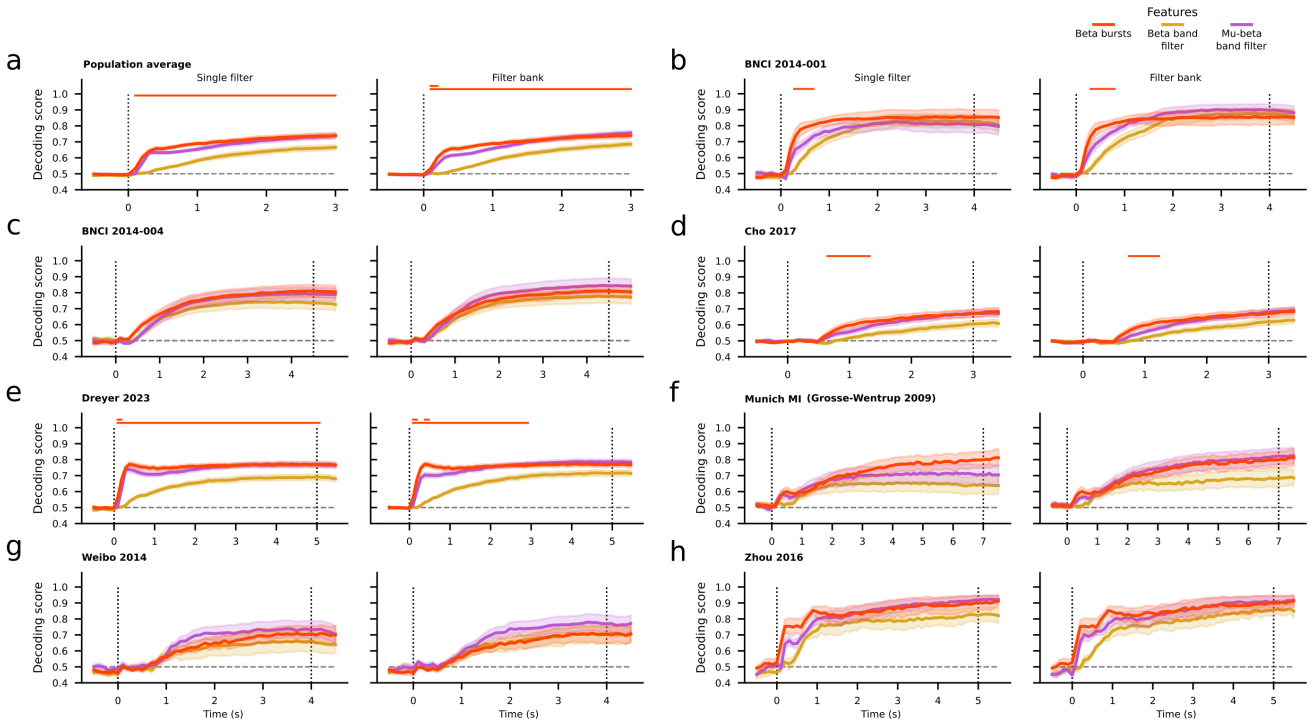

Fig. 2. (a) Population average, time-resolved decoding score, and standard error for the beta burst convolution (red), beta band (yellow), and mu-beta band (purple) filtering pipelines using an incremental window. Due to the different duration of the task per dataset, we restricted the time to the minimum trial period corresponding to 3 seconds. (b–h) Average, time-resolved decoding score and standard error per dataset of the same features using an incremental window. For each panel, the left subplot depicts the decoding results obtained using a single filter, while the right subplot depicts the results based on a filter bank technique. The beta burst results are the same for the pair of each panel. The horizontal dashed line corresponds to the expected chance level. Vertical dotted lines represent the onset and end of the trial period of each dataset. The two horizontal lines on the top of each subplot show the results of the two pair-wise permutation cluster tests, that is, between the beta bursts and the beta band (bottom line) or mu-beta band (top line) filtering technique respectively, with correction for multiple comparisons at a significance level of 0.05. At any time point, each line is color-coded so as to indicate which feature produces, on average, better results. A lack of color at any given time point indicates no statistically significant differences between the compared features.

outperformed the single filter and filter bank techniques early after the beginning of a trial (Fig. 2a). On the dataset level, this was true for the BNCI 2014-001 and Dreyer datasets (Fig. 2b, e). For the rest of the datasets, differences varied depending on the filtering technique. Notably, in the mu-beta band, both filtering techniques produced higher decoding scores than beta bursts for the Weibo 2014 dataset (Fig. 2g). A similar pattern was also observed when using a sliding window (Supplementary Fig. 3a–h). The permutation tests between the beta burst features and the mu-beta filtering techniques revealed only small clusters on the population level, as well for the Dreyer 2023 dataset. We found that beta bursts improve classification scores over the mu-band filtering techniques on the population level and 4/7 (2/7) datasets when using an incremental (sliding) window, with small clusters of statistically significant differences on the population level and one dataset only when using an incremental window.

Finally, comparisons between beta burst convolution and mu filtering results showed an improvement when using an incremental window. No clusters of statistically significant differences were revealed when comparing beta bursts to single-filter mu band power on the population level, but beta bursts slightly improved decoding on the population level and for datasets BNCI 2014-001, BNCI 2014-004, and Zhoud 2016 (Supplementary Fig. 4a–c). No differences were found on the population level when comparing beta bursts to the filter bank technique, but on the dataset level the beta bursts score was better for the BNCI 2014-001 dataset (Supplementary Fig. 4b) and conversely worse for the Weibo 2014 dataset (Supplementary Fig. 4g) based on cluster permutation tests. Comparisons of results when using a sliding window approach did not reveal any differences (Supplementary Fig. 5).

3.2. Information transfer rate

For all datasets we computed the information transfer rate (ITR) in order to quantify the difference between all classification features in terms of the decoding speed-accuracy trade-off (see Section 2). On the population level, beta bursts provided a higher ITR than either beta band filtering technique across the whole trial (Fig. 3a). On the dataset level, the same pattern was observed for the Dreyer 2023 dataset (Fig. 3e). Moreover, beta bursts ITR was higher than any beta band filtering early after trial onset for the BNCI 2014-001, Munich MI (Grosse-Wentrup 2009), and Zhou 2016 datasets, and later for the Cho 2017 dataset. No differences between the features were observed in the case of BNCI 2014-004 dataset, whereas beta bursts resulted in the lowest ITR for the Weibo 2014 dataset (Fig. 3b–h). Permutation cluster tests revealed a significant difference between beta bursts and either filtering technique in the beta band on the population level, and for most of the time for the Dreyer 2023 dataset. A cluster after the trial onset was found for the BNCI 2014-001 dataset, and no clusters were found for the rest of the datasets. When using a sliding window approach, beta bursts provided a higher ITR than either beta band filtering technique on the population level early after the beginning of the trial and toward its end highlighted by the presence of a cluster (Supplementary Fig. 6a). A significant difference was also found for the Dreyer 2023 dataset after the trial onset (Supplementary Fig. 6e). For datasets BNCI 2014-001, Cho 2017, Dreyer 2023, and Zhou 2016 we observed a higher ITR for beta bursts compared to beta band filtering mainly after the trial onset, whereas for the rest of the datasets either feature resulted in equivalent ITRs (Supplementary Fig. 6b–h). No significant clusters were found for any of these datasets. In summary, irrespective of the windowing method beta bursts resulted in higher ITR than beta power on the population level and for 5/7 datasets with clusters arising on the population level and 2/7 datasets.

Regarding the comparison between beta bursts and the mu-beta filtering techniques, ITR was higher for the former on the population level as well as datasets BNCI 2014-001, Cho 2017, Dreyer 2023, Munich MI (Grosse-Wentrup 2009), and Zhou 2016 shortly after the trial onset, especially when adopting the filter bank method. No differences were observed for the BNCI 2014-004 dataset. The mu-band filter bank technique produced higher ITR than beta bursts period in the case of the Weibo 2014 dataset (Fig. 3a–h). The results were similar when using a sliding window (Supplementary Fig. 6a–h). On the population level, cluster-based permutations tests revealed a significant difference between the beta bursts features and the filter bank in the mu-beta band using either an incremental or a sliding window approach, but no significant clusters when comparing the beta bursts to the single filter in the mu-beta band (Fig. 3a; Supplementary Fig. 6a). Similar clusters of significant differences between the features were found only for the Dreyer 2023 dataset with an incremental window (Fig. 3e; Supplementary Fig. 6e). Overall, beta bursts yielded higher ITR than mu-beta power on the population level and 4/7 datasets regardless of the windowing technique. Permutation cluster tests revealed improvements attributable to beta bursts compared to the filter bank technique on the population level, and for one dataset when using an incremental time window.

3.3. Statistical analysis

We used linear mixed models to quantify the differences in maximum decoding score, latency to achieve the

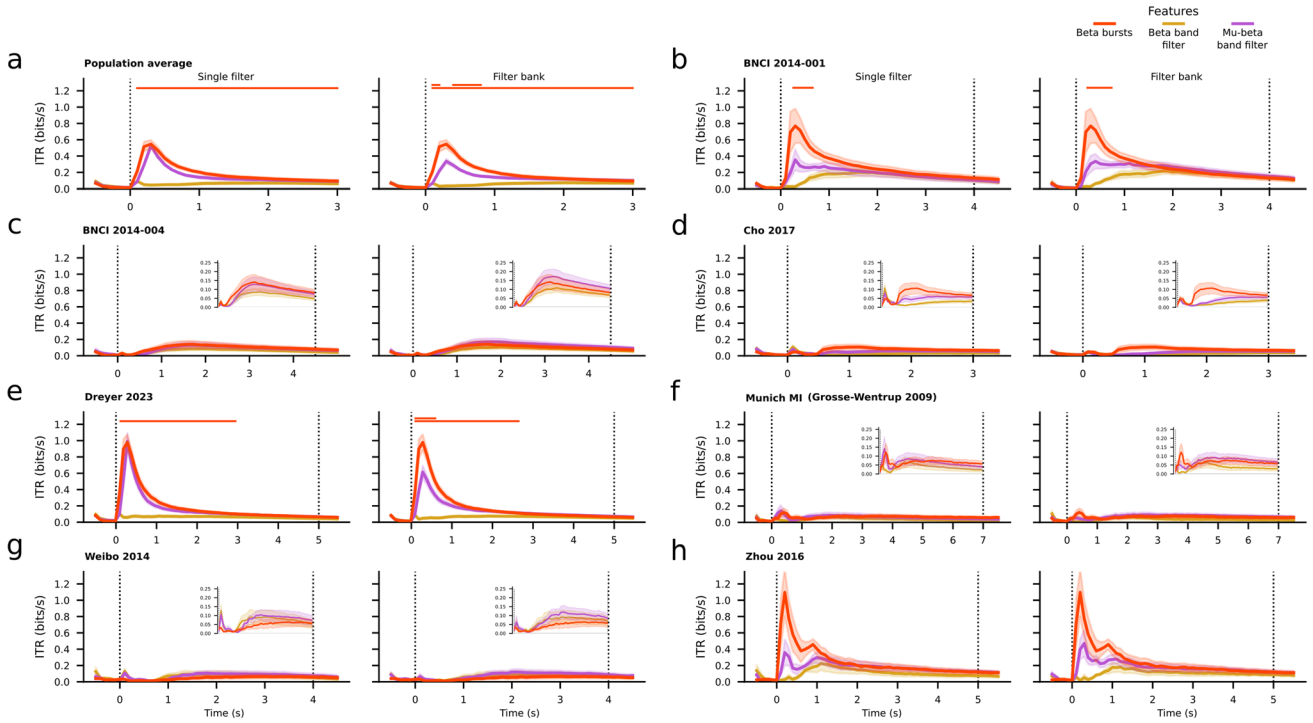

Fig. 3. (a) Population average, time-resolved information transfer rate (ITR), and standard error for the beta burst convolution (red), beta band (yellow), and mu-beta band (purple) filtering pipelines using an incremental window. Due to the different duration of the task per dataset, we restricted the time to the minimum trial period corresponding to 3 seconds. (b–h) Average, time-resolved information transfer rate (ITR), and standard error per dataset of the same features using an incremental window. For each panel, the left subplot depicts the ITR results obtained using a single filter, while the right subplot depicts the results based on a filter bank technique. The beta burst results are the same for the pair of each panel. Vertical dotted lines represent the onset and end of the trial period of each dataset. The two horizontal lines on the top of each subplot show the results of the two pair-wise permutation cluster tests, that is, between the beta bursts and the beta band (bottom line) or mu-beta band (top line) filtering technique respectively, with correction for multiple comparisons at a significance level of 0.05. At any time point, each line is color-coded so as to indicate which feature produces, on average, better results. A lack of color at any given time point indicates no statistically significant differences between the compared features.

maximum score, maximum ITR, and latency to the maximum ITR per feature (see Section 2) using both the incremental and sliding windows (Fig. 4; Supplementary Fig. 7).

On the population level, the maximum classification scores for the beta bursts technique, filtering in the beta band using a single filter, filtering in the mu band using a single filter, and filter bank in the beta or mu and beta bands using an incremental time window were 0.832 ± 0.066, 0.755 ± 0.065, 0.827 ± 0.066, 0.734 ± 0.066, and 0.819 ± 0.066 (Fig. 4a). The time required to reach each of these decoding scores (latency) was 2.26 ± 0.91, 3.04 ± 0.90, 2.96 ± 0.90, 2.50 ± 0.90, and 2.44 ± 0.91 seconds (Fig. 4c), respectively. The maxima of the ITR before applying the logarithmic transformation (see Section 2) per feature were 0.6443 ± 0.207, 0.0554 ± 0.207, 0.3531 ± 0.0206, 0.0667 ± 0.206, and 0.5241 ± 0.207 bits per second (Fig. 4b). The corresponding average latencies before the logarithmic transformation were 0.827 ± 0.203, 1.316 ± 0.204, 1.182 ± 0.203, 1.064 ± 0.201, and 0.945 ± 0.203 seconds (Fig. 4d). Regarding the analysis based on a sliding window, the maximum classification scores were 0.816 ± 0.050, 0.753 ± 0.050, 0.810 ± 0.050, 0.753 ± 0.050, and 0.818 ± 0.050 respectively (Supplementary Fig. 7a). The latencies were 2.03 ± 0.23, 2.45 ± 0.22, 2.19 ± 0.23, 2.49 ± 0.24, and 2.22 ± 0.23 seconds (Supplementary Fig. 7c). Before applying the logarithmic transformation, the ITR maxima were 0.694 ± 0.180, 0.170 ± 0.178, 0.413 ± 0.177, 0.206 ± 0.182, and 0.533 ± 0.179 bits per second (Supplementary Fig. 7b), and the corresponding latencies were 0.575 ± 0.162, 0.840 ± 0.161, 0.796 ± 0.160, 0.743 ± 0.161, and 0.701 ± 0.162 seconds (Supplementary Fig. 7d).

Across all datasets, the maximum classification accuracy of the beta bursts technique when using an incremental window was significantly higher than that of the beta band single filter and filter bank pipelines ($X^2(4) = 326.81$, $t(24587436) = 10.697$, $p < 0.001$ and $t(24548972) = 13.705$, $p < 0.001$ respectively), but did not differ significantly from either technique exploiting both the mu and beta bands ($t(24904394) = 0.637$, $p = 0.9691$ and $t(24049399) = 1.777$,

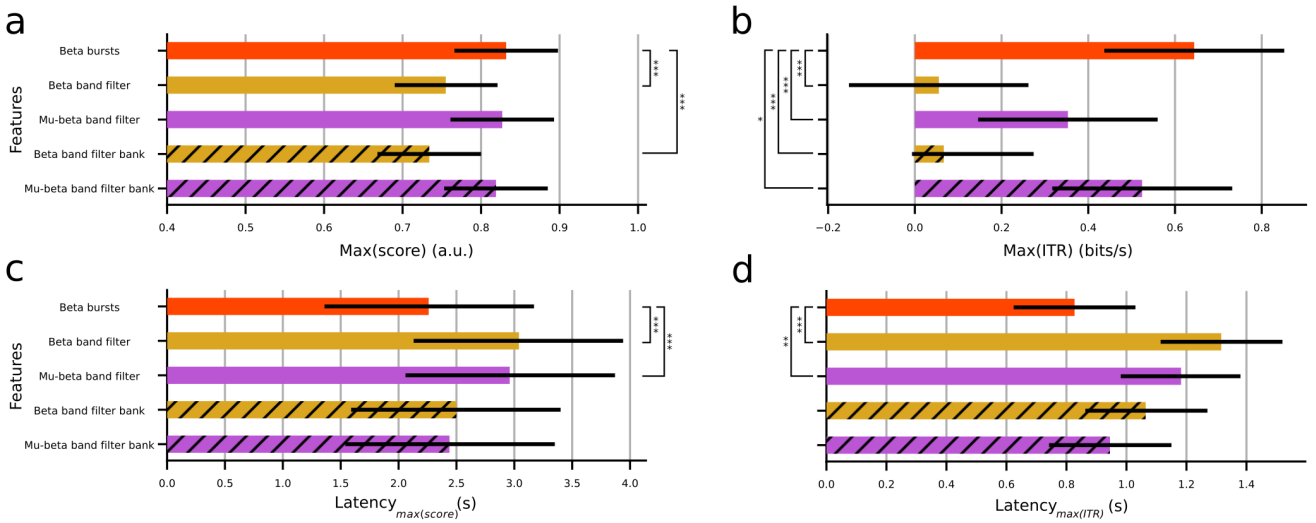

Fig. 4. Population-level statistical analysis based on linear mixed models when using an incremental window per feature. (a) Average maximum decoding score. (b) Average maximum ITR. (c) Average latency to reach the maximum decoding score. (d) Average latency to reach the maximum ITR. Error bars show 95% confidence intervals. Hatches indicate the use of a filter bank technique. Asterisks indicate statistically significant differences among pairwise comparisons of the beta bursts and the rest of the features (*p < 0.05. **p < 0.01, ***p < 0.001). A lack of asterisks implies no statistically significant differences. Note that the log transform of the maximum ITR and latency to maximum ITR were used for the statistical analysis (see Section 2), but panels (b and d) depict results before applying the transformation for ease of comparisons with panels (a and c) respectively.

p = 0.3873). The latency to achieve the maximum score was significantly lower for the beta burst convolution pipeline compared to both the single filtering techniques in the beta and mu-beta bands ($X^2(4)$ = 62.508, t(24698263) = -6.361, p < 0.001 and t(25032435) = -5.769, p < 0.001), but did not differ significantly compared to the corresponding filter bank techniques (t(24649522) = -1.926, p = 0.3034 and t(24151454) = -1.488, p = 0.5703). The logarithmic transform of the maximum ITR for the beta bursts technique was significantly higher than the single filtering and filter bank techniques in both the beta and mu-beta bands ($X^2(4)$ = 309.58, t(24722157) = 14.0967, p < 0.001, t(24671284) = 12.904, p < 0.001 and t(25060057) = 5.127, p < 0.001, t(24173608) = 2.909, p = 0.0298). The logarithmic transform of the latency to achieve maximum ITR was significantly lower for the beta bursts technique compared to either single filtering pipeline in the beta and mu-beta bands ($X^2(4)$ = 40.75, t(24777354) = -5.863, p < 0.001 and t(25130735) = -3.885, p = 0.001), but did not significantly differ compared to the filter bank method in either band (t(24721433) = -2.071, p = 0.2329 and t(24227058) = -1.545, p = 0.5329).

When using a sliding window, across all datasets the maximum classification accuracy of the beta bursts technique was significantly higher than that of the beta band single filter and filter bank pipelines ($X^2(4)$ = 237.95, t(24582761) = 10.072, p < 0.001 and t(24544732) = 10.055, p < 0.001 respectively), but did not differ significantly from either technique exploiting both the mu and beta bands (t(24898964) = 0.956, p = 0.8748 and t(24045211) = -0.418, p = 0.9936). Similarly, the latency to achieve the maximum score was significantly lower for the beta burst convolution pipeline compared to either filtering technique in the beta band ($X^2(4)$ = 25.552, t(24736767) = -3.890, p < 0.001 and t(24684274) = -4.281, p < 0.001), but did not differ significantly compared to the mu-beta band (t(25086359) = -1.467, p = 0.5840 and t(24189739) = -1.762, p = 0.3961). The logarithmic transform of the maximum ITR for the beta bursts technique was significantly higher than both filtering techniques in the beta band and the single filtering in the mu-beta band ($X^2(4)$ = 162.26, t(24732475) = 10.236, p < 0.001, t(24680636) = 9.172, p < 0.001 and t(25072582) = 4.499, p < 0.001) but did not significantly differ from the mu-beta filter bank (t(24183763) = 1.665, p = 0.4559). The logarithmic transform of the latency to achieve maximum ITR was significantly lower for the beta bursts technique compared to either single filtering pipeline in the beta and mu-beta bands ($X^2(4)$ = 13.151, t(24808114) = -3.069, p = 0.0183 and t(25164334) = -3.029, p = 0.0207), but did not significantly differ compared to the filter bank method in either band (t(24749694) = -1.796, p = 0.3756 and t(24255336) = -1.296, p = 0.6937).

4. DISCUSSION

Standard techniques for analyzing meso- and macroscale neural signals recorded during the execution or

imagination of movements typically rely on signal power metrics assuming that relevant changes in brain signals are reflected in amplitude modulation (Alayrangues et al., 2019; Kilavik et al., 2013; Pfurtscheller, 1981; Pfurtscheller et al., 1996, 1997; Pfurtscheller & Lopes da Silva, 1999). However, there has recently been a considerable paradigm shift toward considering transient signal features on the single-trial level (Chen et al., 2021; Coleman et al., 2024; Jones, 2016; Little et al., 2019; Lundqvist et al., 2016, 2024; Rayson et al., 2023; Shin et al., 2017; Soh et al., 2021; Szul et al., 2023; Torrecillos et al., 2018; Vigué-Guix & Soto-Faraco, 2023; Wessel, 2020). Therefore, considering that computational models describing the neuronal generators of specific burst waveform shapes (Bonaiuto et al., 2021; Sherman et al., 2016; Szul et al., 2023) offer an improved theoretical interpretability of the observed signal modulations, applications leveraging such signal characteristics, like beta bursts, could potentially benefit from incorporating recent neuroscience findings (Papadopoulos et al., 2022).

In this work, we analyzed the activity of seven open EEG MI datasets and focused on developing a streamlined process for incorporating beta bursts into a BCI pipeline. We used a simple pre-processing algorithm in order to reject noisy trials based on amplitude thresholds before detecting beta bursts, but the impact of more sophisticated algorithms like independent component analysis on burst detection could be explored in the future. Then, we defined a modulation index I_m which allowed us to identify beta burst waveforms whose rate is expected to be modulated due to task demands. This was based on the assumption that maximal modulations of the average waveform shape along specific PCA components are the result of a net imbalance of the rates of bursts with different shapes driven by task demands. PCA constitutes a mathematically tractable and interpretable way of analyzing the diversity of beta burst waveform shapes. However, by definition it imposes, to some extent, orthogonality in the frequency content of the kernels, a property which may not be desirable. Other supervised dimensionality reduction algorithms, especially those designed for analyzing time series, could better disentangle the waveforms by imposing different constraints, for example, taking into account trial labels, and their potential advantages remain to be studied. We also note that this index only used beta burst waveforms originating from channels C3 and C4 (or equivalent). Our assumption was that the channels localization should allow for signals which are sufficiently informative of the binary "left hand" versus "right hand" MI task. Future work can explore a more principled way to include data from multiple channels.

We used these waveforms as kernels to convolve the raw signals in the time domain. We chose to keep the number of kernels and the method for extracting them fixed based on insights from a previous study (Papadopoulos et al., 2024), but future work could employ a formal hyperparameter search so as to maximize classification accuracy. Similarly, we did not check for any redundancy in the convolved signals due to selection of similarly shaped kernels, a point which could be addressed by another dimensionality reduction algorithm. The implementation of the convolution is virtually as computationally efficient as any filtering technique. However, we note that the proposed methodology assumes the existence of data that can be analyzed offline in order to first find the relevant beta burst waveforms to use as kernels. Moreover, these data need to be clean of artifacts as the beta burst detection algorithm may fail to detect transient activity in the presence of high-power oscillations, instead detecting only the latter. For this reason, we believe that the superlets algorithm is the only time-frequency decomposition technique providing adequate time and frequency resolution in order to determine if the data are clean and to extract burst waveforms.

This data-driven, neurophysiology-informed filtering of the signals resulted in a proxy of waveform-resolved burst rate per kernel. We also performed a standard filtering in the mu (6–15 Hz) band, beta (15–30 Hz) band, or a wider frequency range encompassing both the mu and beta (6–30 Hz) bands. Finally, we used CSP to extract spatial features for classification. We showed that classification scores can be improved compared to a standard power-based analysis of the beta band activity, requiring briefer recordings to do so and that, without explicitly considering the mu (6–15 Hz) band activity in our beta bursts pipeline, the corresponding classification scores are equivalent to scores of state-of-the-art approaches again needing shorter recordings. Further, the filter bank-based analysis allowed us to verify that the decoding improvements were not simply the result of an increase in number of spatial features used for classification. Instead, beta burst waveforms are more informative of the underlying MI task on the population level than beta band power, and equally informative to standard power-based techniques that take into account mu activity modulations.

A possible explanation for this result is that beta burst kernels also capture slower modulations of the underlying activity. Beta and mu band modulations during MI tasks involve overlapping cortical networks and have equivalent time horizons (Neuper et al., 2006; Pfurtscheller & Neuper, 2001; Seeber et al., 2016). The actual signal properties and/or underlying mechanisms that would explain why beta burst waveforms perform similarly to oscillatory mu band power remain to be studied. As such, we have opted not to perform a formal comparison of the

beta burst features to mu band power. However, one hypothesis is that our definition of the mu band frequency range overlaps—at least partially—with what has been described as lower beta frequency (Kilavik et al., 2012; Lotte, 2014; Lotte & Rimbert, 2022; Schmidt et al., 2019). Future work could explore the incorporation of novel mu band features that characterize time-resolved oscillatory waveform changes (Cole & Voytek, 2019; Giehl & Siegel, 2024; Vigué-Guix & Soto-Faraco, 2023), or a combination of mu power and beta burst features using more sophisticated classifiers or ensemble methods. We also note that the use of alternative classifiers can potentially affect the beta burst results reported here. Although the combination of CSP and LDA is known to produce reliable results (Carrara & Papadopoulo, 2024; Jayaram & Barachant, 2018), a formal comparison of multiple classifiers would be necessary in order to optimize performance and/or ITR, especially for online applications.

By employing both an incremental and a sliding window strategy for classification, we can speculate on the observed differences of decoding scores across classification features and datasets. First, it appears that MI does not begin right after the go cue in all datasets but can be delayed possibly due to differences in the task design or the instructions given to the participants. Second, relatively sustained decoding performances when using a sliding window were translated into slow increases of those performances when using an incremental window. In contrast, a drop in performance when using a sliding window was reflected in a plateau when using an incremental window. Taken together, these observations imply that finding an optimal decoding time window, especially for online paradigms, is not trivial and depends not only on the selected classification features or algorithm but also on experimental design variables.

In order to assess the trade-off between decoding accuracy and speed, we used the classification scores obtained by implementing each pipeline and computed the corresponding ITR. By definition, given a fixed number of classes ITR increases either by reducing recording time or by increasing decoding score (or a combination of the two). This means that when comparing different features and/or algorithms, ITR will indicate which one is faster assuming equivalent classification scores, or which one performs best assuming equivalent recording times. We showed a statistically significant increase of the maximum ITR achieved using the beta burst kernel filtering compared to any other method, and a statistically significant decrease of the time needed to achieve this value compared to single filters. These results are in accordance with previous studies that have showed the specificity of waveform-resolved burst rate which captures subtle changes on the single-trial level not necessarily reflected in signal power and overall burst rate (Papadopoulos et al., 2024; Rayson et al., 2023; Szul et al., 2023), due to slower amplitude modulation and averaging over distinct processes respectively. The results suggest that, by retaining or improving the precision of command issuing while increasing its speed, beta bursts could be particularly relevant for BCI applications that aim to minimize the recording time required before issuing a command like in the case of real-time decoding of a switch control, although the self-paced nature of such applications still poses a considerable challenge (Carrara & Papadopoulo, 2024).

Among the datasets analyzed in this study, decoding and ITR results of the Weibo 2014 were noticeably different. This dataset is to some degree contaminated by high-frequency noise even following pre-processing and, compared to what we have observed for the rest of the datasets, is characterized by a smaller number of detected bursts the majority of which last longer (more than 5 cycles) and have higher amplitude. The reduced variability in the detected bursts is also reflected in the smaller number of PCA components that explain at least 90% of the variance. We presume that these recordings are mostly composed of oscillatory rather than burst activity. Therefore, the proposed, burst-based approach, despite being able to capture and quantify modulations of signal amplitude, is sub-optimal for this dataset.

This study focused on incorporating recent neurophysiology insights, specifically task dependent waveform-specific modulation of beta burst rates, in a pipeline for decoding EEG signals during imagined movements. We proposed a simple and computationally efficient algorithm that leverages beta burst waveforms and transforms brain recordings in a way that is compatible with other widely adopted algorithms. We demonstrated that classification results based on beta bursts are superior to results based on beta band power alone, and are on-par with power-based results that take into account the mu band. By computing the information transfer rate, we showed that, often, features based on beta bursts significantly improve the decoding speed-accuracy trade-off. We also verified this finding using a sliding window decoding technique, a fact which further suggests the feasibility for online decoding with this approach. Taking everything into account, we believe that these findings can serve as an important step in the direction of improving online BCI decoding paradigms.

DATA AND CODE AVAILABILITY

All data are freely available via the MOABB project and the open access repository Zenodo at https://zenodo.org/records/8089820. All scripts necessary for reproducing

the results of this article are available at the following public repository: https://gitlab.com/sotpapad/bebopbci.

AUTHOR CONTRIBUTIONS

S.P., J.J.B., and J.M. conceptualized the manuscript. S.P. drafted the manuscript and performed the analysis. All authors contributed to manuscript revision, read, and approved the submitted version.

FUNDING

S.P., L.D., M.C., J.J.B., and J.M. are supported by the French National Research Agency (ANR) project HiFi (2020–2024, ANR-20-CE17-0023). M.J.S. and J.J.B. are supported by the European Research Council (ERC) under the European Union's Horizon 2020 Research and Innovation Programme (ERC consolidator Grant 864550 to J.J.B.). This work was performed within the framework of the LABEX CORTEX (ANR-11LABX-0042) of Université de Lyon, within the program "Investissements d'Avenir" (decision no 2019-ANR-LABX-02) operated by the French National Research Agency (ANR).

DECLARATION OF COMPETING INTEREST

All authors declare no competing interests.

SUPPLEMENTARY MATERIALS

Supplementary material for this article is available with the online version here: https://doi.org/10.1162/imag_a_00391.

REFERENCES

Alayrangues, J., Torrecillos, F., Jahani, A., & Malfait, N. (2019). Error-related modulations of the sensorimotor post-movement and foreperiod beta-band activities arise from distinct neural substrates and do not reflect efferent signal processing. *Neuroimage*, *184*, 10–24. https://doi.org/10.1016/j.neuroimage.2018.09.013

Aristimunha, B., Carrara, I., Guetschel, P., Sedlar, S., Rodrigues, P., Sosulski, J., Narayanan, D., Bjareholt, E., Quentin, B., Schirrmeister, R. T., Kalunga, E., Darmet, L., Gregoire, C., Abdul Hussain, A., Gatti, R., Goncharenko, V., Thielen, J., Moreau, T., Roy, Y., … Chevallier, S. (2023). Mother of all BCI Benchmarks. *Zenodo*. https://doi.org/10.5281/zenodo.10034224

Arslan, S. S., & Sinha, P. (2024). Information transfer rate in BCIs: Towards tightly integrated symbiosis. *Biomed Signal Process Control*, *87*, 105466. https://doi.org/10.1016/j.bspc.2023.105466

Bates, D., Mächler, M., Bolker, B. M., & Walker, S. C. (2015). Fitting linear mixed-effects models using lme4. *J Stat Softw*, *67*(1), 1–48. https://doi.org/10.18637/jss.v067.i01

Blankertz, B., Kawanabe, M., Tomioka, R., Hohlefeld, F., Müller, K.-R., & Nikulin, V. (2007). Invariant common spatial patterns: Alleviating nonstationarities in brain-computer interfacing. In Platt, J., Koller, D., Singer, Y., & Roweis, S. (Eds.), *Advances in neural information processing systems*. Curran Associates, Inc. https://proceedings.neurips.cc/paper_files/paper/2007/file/6aab1270668d8cac7cef2566a1c5f569-Paper.pdf

Bonaiuto, J. J., Little, S., Neymotin, S. A., Jones, S. R., Barnes, G. R., & Bestmann, S. (2021). Laminar dynamics of high amplitude beta bursts in human motor cortex. *Neuroimage*, *242*, 118479. https://doi.org/10.1016/j.neuroimage.2021.118479

Brodu, N., Lotte, F., & Lécuyer, A. (2011). Comparative study of band-power extraction techniques for Motor Imagery classification. In *IEEE SSCI 2011—Symp Ser Comput Intell—CCMB 2011 2011 IEEE Symp Comput Intell Cogn Algorithms, Mind, Brain* (pp. 95–100). IEEE. https://doi.org/10.1109/CCMB.2011.5952105

Bruns, A. (2004). Fourier-, Hilbert- and wavelet-based signal analysis: Are they really different approaches? *J Neurosci Methods*, *137*, 321–332. https://doi.org/10.1016/j.jneumeth.2004.03.002

Carrara, I., & Papadopoulo, T. (2024). Pseudo-online framework for BCI evaluation: A MOABB perspective using various MI and SSVEP datasets. *J Neural Eng*, *21*, 016003. https://doi.org/10.1088/1741-2552/ad171a

Chen, Y. Y., Lambert, K. J. M, Madan, C. R., & Singhal, A. (2021). Mu oscillations and motor imagery performance: A reflection of intra-individual success, not inter-individual ability. *Hum Mov Sci*, *78*, 1–12. https://doi.org/10.1016/j.humov.2021.102819

Cho, H., Ahn, M., Ahn, S., Kwon, M., & Jun, S. C. (2017). EEG datasets for motor imagery brain-computer interface. *Gigascience*, *6*, 1–8. https://doi.org/10.1093/gigascience/gix034

Cole, S., & Voytek, B. (2019). Cycle-by-cycle analysis of neural oscillations. *J Neurophysiol*, *122*, 849–861. https://doi.org/10.1152/JN.00273.2019

Coleman, S. C., Seedat, Z. A., Pakenham, D. O., Quinn, A. J., Brookes, M. J., Woolrich, M. W., & Mullinger, K. J. (2024). Post-task responses following working memory and movement are driven by transient spectral bursts with similar characteristics. *Hum Brain Mapp*, *45*(7), e26700. https://doi.org/10.1002/hbm.26700

de Cheveigné, A. (2020). ZapLine: A simple and effective method to remove power line artifacts. *Neuroimage*, *207*, 116356. https://doi.org/10.1016/j.neuroimage.2019.116356

Dreyer, P., Roc, A., Pillette, L., Rimbert, S., & Lotte, F. (2023). A large EEG database with users' profile information for motor imagery brain-computer interface research. *Sci Data*, *10*, 1–14. https://doi.org/10.1038/s41597-023-02445-z

Enz, N., Ruddy, K. L., Rueda-Delgado, L. M., & Whelan, R. (2021). Volume of β-bursts, but not their rate, predicts successful response inhibition. *J Neurosci*, *41*, 5069–5079. https://doi.org/10.1523/JNEUROSCI.2231-20.2021

Fox, J., & Weisberg, S. (2019). *An R Companion to Applied Regression* (3rd ed.). Sage. https://doi.org/10.32614/cran.package.car

Giehl, J., & Siegel, M. (2024). Spectral waveform analysis dissociates human cortical alpha rhythms. *bioRxiv* 1–11. https://doi.org/10.1101/2024.03.16.585296

Gordon, E. M., Chauvin, R. J., Van, A. N., Rajesh, A., Nielsen, A., Newbold, D. J., Lynch, C. J., Seider, N. A., Krimmel, S. R., Scheidter, K. M., Monk, J., Miller, R. L., Metoki, A., Montez, D. F., Zheng, A., Elbau, I., Madison, T., Nishino, T., Myers, M. J., … Dosenbach, N. U. F. (2023). A somato-cognitive action network alternates with effector regions in motor cortex. *Nature*, *617*, 351–359. https://doi.org/10.1038/s41586-023-05964-2

Gramfort, A., Luessi, M., Larson, E., Engemann, D. A., Strohmeier, D., Brodbeck, C., Goj, R., Jas, M., Brooks, T., Parkkonen, L., & Hämäläinen, M. (2013). MEG and EEG data analysis with MNE-Python. *Front Neurosci*, *7*, 267. https://doi.org/10.3389/fnins.2013.00267

Grosse-Wentrup, M., Liefhold, C., Gramann, K., & Buss, M. (2009). Beamforming in noninvasive brain–computer interfaces. *IEEE Trans Biomed Eng*, *56*, 1209–1219. https://doi.org/10.1109/TBME.2008.2009768

Hannah, R., Muralidharan, V., Sundby, K. K., & Aron, A. R. (2020). Temporally-precise disruption of prefrontal cortex informed by the timing of beta bursts impairs human action-stopping. *Neuroimage*, *222*, 117222. https://doi.org/10.1016/j.neuroimage.2020.117222

Harris, C. R., Millman, K. J., van der Walt, S. J., Gommers, R., Virtanen, P., Cournapeau, D., Wieser, E., Taylor, J., Berg, S., Smith, N. J., Kern, R., Picus, M., Hoyer, S., van Kerkwijk, M. H., Brett, M., Haldane, A., del Río, J. F., Wiebe, M., Peterson, P., … Oliphant, T. E. (2020). Array programming with NumPy. *Nature*, *585*, 357–362. https://doi.org/10.1038/s41586-020-2649-2

Herman, P., Prasad, G., McGinnity, T. M., & Coyle, D. (2008). Comparative analysis of spectral approaches to feature extraction for EEG-based motor imagery classification. *IEEE Trans Neural Syst Rehabil Eng*, *16*, 317–326. https://doi.org/10.1109/TNSRE.2008.926694

Jas, M., Engemann, D. A., Bekhti, Y., Raimondo, F., Gramfort, A., Gramfort, A., Automated, A., & Engemann, D. A. (2017). Autoreject: Automated artifact rejection for MEG and EEG data. *Neuroimage*, *159*, 417–129. https://doi.org/10.1016/j.neuroimage.2017.06.030

Jayaram, V., & Barachant, A. (2018). MOABB: Trustworthy algorithm benchmarking for BCIs. *J Neural Eng*, *15*(6), 066011. https://doi.org/10.1088/1741-2552/aadea0

Jones, S. R. (2016). When brain rhythms aren't 'rhythmic': Implication for their mechanisms and meaning. *Curr Opin Neurobiol*, *40*, 72–80. https://doi.org/10.1016/j.conb.2016.06.010

Kilavik, B. E., Ponce-Alvarez, A., Trachel, R., Confais, J., Takerkart, S., & Riehle, A. (2012). Context-related frequency modulations of macaque motor cortical LFP beta oscillations. *Cereb Cortex*, *22*, 2148–2159. https://doi.org/10.1093/cercor/bhr299

Kilavik, B. E., Zaepffel, M., Brovelli, A., MacKay, W. A., & Riehle, A. (2013). The ups and downs of beta oscillations in sensorimotor cortex. *Exp Neurol*, *245*, 15–26. https://doi.org/10.1016/j.expneurol.2012.09.014

Kobler, R. J., Almeida, I., Sburlea, A. I., & Müller-Putz, G. R. (2020). Using machine learning to reveal the population vector from EEG signals. *J Neural Eng*, *17*, 026002. https://doi.org/10.1088/1741-2552/ab7490

Koles, Z. J. (1991). The quantitative extraction and topographic mapping of the abnormal components in the clinical EEG. *Electroencephalogr Clin Neurophysiol*, *79*, 440–447. https://doi.org/10.1016/0013-4694(91)90163-X

Langford, Z. D., Procyk, E., & Wilson, C. R. E. (2023). Frontal oscillatory beta bursts have rhythmically distinct regimes with differing functional relevance. *bioRxiv* 1–19. https://doi.org//doi.org/10.1101/2023.11.13.566594

Leeb, R., Lee, F., Keinrath, C., Scherer, R., Bischof, H., & Pfurtscheller, G. (2007). Brain-computer communication: Motivation, aim, and impact of exploring a virtual apartment. *IEEE Trans Neural Syst Rehabil Eng*, *15*, 473–482. https://doi.org/10.1109/TNSRE.2007.906956

Lenth, R. V. (2023). emmeans: Estimated Marginal Means, *aka Least-Squares Means*. https://doi.org/10.32614/cran.package.emmeans

Little, S., Bonaiuto, J., Barnes, G., & Bestmann, S. (2019). Human motor cortical beta bursts relate to movement planning and response errors. *PLoS Biol*, *17*, 1–30. https://doi.org/10.1371/journal.pbio.3000479

Lotte, F. (2014). A tutorial on EEG signal-processing techniques for mental-state recognition in brain-computer interfaces. In E. Miranda & J. Castet (Eds.), *Guid to brain-computer music interfacing* (pp. 133–161). Springer. https://doi.org/10.1007/978-1-4471-6584-2_7

Lotte, F., Bougrain, L., Cichocki, A., Clerc, M., Congedo, M., Rakotomamonjy, A., & Yger, F. (2018). A review of classification algorithms for EEG-based brain-computer interfaces: A 10 year update. *J Neural Eng*, *15*(3), 031005. https://doi.org/10.1088/1741-2552/aab2f2

Lotte, F., & Rimbert, S. (2022). How ERD modulations during motor imageries relate to users' traits and BCI performances. In *2022 44th Annual International Conference of the IEEE Engineering in Medicine & Biology Society (EMBC), Glasgow, Scotland, United Kingdom* (pp. 203–207). IEEE. https://doi.org/10.1109/embc48229.2022.9871411

Lundqvist, M., Miller, E. K., Nordmark, J., Liljefors, J., & Herman, P. (2024). Beta: Bursts of cognition. *Trends Cogn Sci*, *xx*, 1–15. https://doi.org/10.1016/j.tics.2024.03.010

Lundqvist, M., Rose, J., Herman, P., Brincat, S., Buschman, T., & Miller, E. (2016). Gamma and beta bursts underlie working memory. *Neuron*, *90*, 152–164. https://doi.org/10.1016/j.neuron.2016.02.028

Makeig, S., Enghoff, S., Jung, T. P., & Sejnowski, T. J. (2000). A natural basis for efficient brain-actuated control. *IEEE Trans Rehabil Eng*, *8*, 208–211. https://doi.org/10.1109/86.847818

Moca V. V., Bârzan, H., Nagy-Dăbâcan, A., & Mureșan, R. C. (2021). Time-frequency super-resolution with superlets. *Nat Commun*, *12*, 1–18. https://doi.org/10.1038/s41467-020-20539-9

Müller-Gerking, J., Pfurtscheller, G., & Flyvbjerg, H. (1999). Designing optimal spatial filters for single-trial EEG classification in a movement task. *Clin Neurophysiol*, *110*, 787–798. https://doi.org/10.1016/S1388-2457(98)00038-8

Natraj, N., Silversmith, D. B., Chang, E. F., & Ganguly, K. (2022). Compartmentalized dynamics within a common multi-area mesoscale manifold represent a repertoire of human hand movements. *Neuron*, *110*, 154.e12–174.e12. https://doi.org/10.1016/j.neuron.2021.10.002

Neuper, C., Wörtz, M., & Pfurtscheller, G. (2006). Chapter 14 ERD/ERS patterns reflecting sensorimotor activation and deactivation. *Prog Brain Res*, *159*, 211–222. https://doi.org/10.1016/S0079-6123(06)59014-4

Papadopoulos, S., Bonaiuto, J., & Mattout, J. (2022). An impending paradigm shift in motor imagery based brain-computer interfaces. *Front Neurosci*, *15*, 824759. https://doi.org/10.3389/fnins.2021.824759

Papadopoulos, S., Szul, M. J., Congedo, M., Bonaiuto, J. J., & Mattout, J. (2024). Beta bursts question the ruling power for brain–computer interfaces. *J Neural Eng*, *21*, 16010. https://doi.org/10.1088/1741-2552/ad19ea

Pedregosa, F., Varoquaux, G., Gramfort, A., Michel, V., Thirion, B., Grisel, O., Blondel, M., Prettenhofer, P., Weiss, R., Bubourg, V., Vanderplas, J., Passos, A., Cournapeau, D., Brucher, M., Perrot, M., & Duchesnay, E. (2011). Scikit-learn: Machine Learning in Python. *J Mach Learn Res*, *12*, 2825–2830. https://doi.org/10.3389/fninf.2014.00014

Penfield, W., & Rasmussen, T. (1950). *The cerebral cortex of man: A clinical study of localization of function*. Macmillan. https://psycnet.apa.org/record/1951-01483-000

Pfurtscheller, G. (1981). Central beta rhythm during sensorimotor activities in man. *Electroencephalogr Clin Neurophysiol*, *51*, 253–264. https://doi.org/10.1016/0013-4694(81)90139-5

Pfurtscheller, G., & Berghold, A. (1989). Patterns of cortical activation during planning of voluntary movement. *Electroencephalogr Clin Neurophysiol*, *72*, 250–258. https://doi.org/10.1016/0013-4694(89)90250-2

Pfurtscheller, G., Brunner, C., Schlögl, A., & Lopes da Silva, F. H. (2006). Mu rhythm (de)synchronization and EEG single-trial classification of different motor imagery tasks. *Neuroimage*, *31*, 153–159. https://doi.org/10.1016/j.neuroimage.2005.12.003

Pfurtscheller, G., & Lopes da Silva, F. H. (1999). Event-relared EEG/MEG synchronization and desynchronization: Basic principles. *Clin Neurophysiol*, *110*, 1842–1857. https://doi.org/10.1016/S1388-2457(99)00141-8

Pfurtscheller, G., & Neuper, C. (1997). Motor imagery activates primary sensorimotor area in humans. *Neurosci Lett*, *239*, 65–68. https://doi.org/10.1016/S0304-3940(97)00889-6

Pfurtscheller, G., & Neuper, C. (2001). Motor imagery direct communication. *Proc IEEE*, *89*, 1123–1134. https://doi.org/10.1109/5.939829

Pfurtscheller, G., Neuper, C., Flotzinger, D., & Pregenzer, M. (1997). EEG-based discrimination between imagination of right and left hand movement. *Electroencephalogr Clin Neurophysiol*, *103*, 642–651. https://doi.org/10.1016/S0013-4694(97)00080-1

Pfurtscheller, G., Stancák, A., & Neuper, C. (1996). Post-movement beta synchronization. A correlate of an idling motor area? *Electroencephalogr Clin Neurophysiol*, *98*, 281–293. https://doi.org/10.1016/0013-4694(95)00258-8

Rayson, H., Szul, M. J., El-Khoueiry, P., Debnath, R., Gautier-Martins, M., Ferrari, P. F., Fox, N., & Bonaiuto, J. J. (2023). Bursting with potential: How sensorimotor beta bursts develop from infancy to adulthood. *J Neurosci*, *43*, 8487–8503. https://doi.org/10.1523/JNEUROSCI.0886-23.2023

Sadeghi, S., & Maleki, A. (2019). Accurate estimation of information transfer rate based on symbol occurrence probability in brain-computer interfaces. *Biomed Signal Process Control*, *54*, 101607. https://doi.org/10.1016/j.bspc.2019.101607

Schmidt, R., Ruiz, M. H., Kilavik, B. E., Lundqvist, M., Starr, P. A., & Aron, A. R. (2019). Beta oscillations in working memory, executive control of movement and thought, and sensorimotor function. *J Neurosci*, *39*, 8231–8238. https://doi.org/10.1523/JNEUROSCI.1163-19.2019

Seeber, M., Scherer, R., & Müller-Putz, G. R. (2016). EEG oscillations are modulated in different behavior-related networks during rhythmic finger movements. *J Neurosci*, *36*, 11671–11681. https://doi.org/10.1523/JNEUROSCI.1739-16.2016

Sherman, M. A., Lee, S., Law, R., Haegens, S., Thorn, C. A., & Hämäläinen, M. S. (2016). Neural mechanisms of transient neocortical beta rhythms: Converging evidence from humans, computational modeling, monkeys, and mice. *Proc Natl Acad Sci USA*, *113*(33), E4885–E4894. https://doi.org/10.1073/pnas.1604135113

Shin, H., Law, R., Tsutsui, S., Moore, C. I., & Jones, S. R. (2017). The rate of transient beta frequency events predicts impaired function across tasks and species. *Elife*, *6*, e29086. https://doi.org/10.7554/eLife.29086

Shlens, J. (2014). A tutorial on principal component analysis. *arXiv*. https://doi.org/10.7551/mitpress/3717.003.0017

Soh, C., Hynd, M., Rangel, B. O., & Wessel, J. R. (2021). Adjustments to proactive motor inhibition without effector-specific foreknowledge are reflected in a bilateral upregulation of sensorimotor β-burst rates. *J Cogn Neurosci*, *33*, 784–798. https://doi.org/10.1162/jocn_a_01682

Szul, M. J., Papadopoulos, S., Alavizadeh, S., Daligaut, S., Schwartz, D., Mattout, J., & Bonaiuto, J. J. (2023). Diverse beta burst waveform motifs characterize movement-related cortical dynamics. *Prog Neurobiol*, *228*, 102490. https://doi.org/10.1016/j.pneurobio.2023.102490

Tangermann, M., Müller, K. R., Aertsen, A., Birbaumer, N., Braun, C., Brunner, C., Leeb, R., Mehring, C., Miller, K. J., Müller-Putz, G. R., Nolte, G., Pfurtscheller, G., Preissl, H., Schalk, G., Schlögl, A., Vidaurre, C., Waldert, S., & Blankertz, B. (2012). Review of the BCI competition IV. *Front Neurosci*, *6*, 1–31. https://doi.org/10.3389/fnins.2012.00055

Tharwat, A., Gaber, T., Ibrahim, A., & Hassanien, A. E. (2017). Linear discriminant analysis: A detailed tutorial. *AI Commun*, *30*, 169–190. https://doi.org/10.3233/AIC-170729

Torrecillos, F., Tinkhauser, G., Fischer, P., Green, A. L., Aziz, T. Z., Foltynie, T., Limousin, P., Zrinzo, L., Ashkan, K., Brown, P., & Tan, H. (2018). Modulation of beta bursts in the subthalamic nucleus predicts motor performance. *J Neurosci*, *38*, 8905–8917. https://doi.org/10.1523/JNEUROSCI.1314-18.2018

Vidaurre, C., Kawanabe, M., Von Bünau, P., Blankertz, B., & Müller, K. R. (2011). Toward unsupervised adaptation of LDA for brain-computer interfaces. *IEEE Trans Biomed Eng*, *58*, 587–597. https://doi.org/10.1109/TBME.2010.2093133

Vigué-Guix, I., & Soto-Faraco, S. (2023). Using occipital α-bursts to modulate behaviour in real-time. *Cereb Cortex*, *33*, 9465–9477. https://doi.org/10.1093/cercor/bhad217

Wessel, J. R. (2020). Β-bursts reveal the trial-to-trial dynamics of movement initiation and cancellation. *J Neurosci*, *40*, 411–423. https://doi.org/10.1523/JNEUROSCI.1887-19.2019

West, T. O., Duchet, B., Farmer, S. F., Friston, K. J., & Cagnan, H. (2023). When do bursts matter in the primary motor cortex? Investigating changes in the intermittencies of beta rhythms associated with movement states. *Prog Neurobiol*, *221*, 102397. https://doi.org/10.1016/j.pneurobio.2022.102397

Yi, W., Qiu, S., Wang, K., Qi, H., Zhang, L., Zhou, P., He, F., & Ming, D. (2014). Evaluation of EEG oscillatory patterns and cognitive process during simple and compound limb motor imagery. *PLoS One*, *9*, 1–19. https://doi.org/10.1371/journal.pone.0114853

Zhou, B., Wu, X., Lv, Z., Zhang, L., & Guo, X. (2016). A fully automated trial selection method for optimization of motor imagery based Brain-Computer interface. *PLoS One*, *11*, 1–20. https://doi.org/10.1371/journal.pone.0162657

Zich, C., Quinn, A. J., Bonaiuto, J. J., O'Neill, G., Mardell, L. C., Ward, N. S., & Bestmann, S. (2023). Spatiotemporal organization of human sensorimotor beta burst activity. *Elife*, *12*, e80160. https://doi.org/10.7554/eLife.80160